Scanning tunneling spectroscopy signature of finite-size and connected nanotubes: A tight-binding study

V. Meunier, P. Senet, and Ph. Lambin
Département de Physique, Facultés Universitaires Notre-Dame de la Paix, Rue de Bruxelles 61, B-5000 Namur, Belgium
(Received 5 April 1999)

We present tight-binding-based simulations of the scanning tunneling spectroscopic signal of different types of carbon nanotubes. Capped, finite, and connected nanotubes have been investigated. We have computed scanning tunneling spectroscopy (STS) maps of each nanotube on different parts of the systems for various tip-sample bias potentials. STS reflects the electronic structure, which depends on the arrangement of atoms in the systems, and can be drastically different even for similar geometries. The computations are in good agreement with recently measured STS spectra. Furthermore, the STS spectra of pentagon and heptagon, which are needed for connecting different carbon nanotubes, constitute characteristic marks of topological defects. [S0163-1829(99)09935-X]

Since Iijima's observations in 1991,[1] carbon nanotubes have been the subject of an increasing number of experimental and theoretical studies. Most of them have shown that carbon nanotubes can be considered as nearly perfect objects for the illustration of quantum physics effects.[2] On the other hand, the prospect for industrial applications of these ''ultimate fibers'' remains one of the main concerns of a large number of scientists and nonscientists. For a recent review on the physics and chemistry of carbon nanotubes, see Refs. 3 and 4.

The scanning tunneling microscopic (STM) resolution of carbon nanotubes' atomic structure was accompanied by the confirmation, using scanning tunneling spectroscopy (STS), of the predicted one-dimensional electronic structure of carbon nanotubes.[5–9] Defects affect the physical properties of the nanotubes. In this respect, the identification of topological defects of nanotubes as well as the resolution of the atomic structure of the ending caps is not easily done with STM. For that purpose, STS is more appropriate since it can probe the unique electronic signature of particular geometrical features of carbon nanotubes, such as Stone-Wales defects[10] or ending caps.[7,11]

In a previous work, we accounted for a simple theoretical framework which enabled us to explain, reproduce, and predict STM measurements on carbon nanotubes in a large number of situations.[12] In the present paper, our attention is focused on the STS signature of finite-size nanotubes, cap structures, and topological defects.

Recently, Rubio and co-workers have addressed a theoretical study devoted to STS on finite-length carbon nanotubes.[13] Due to the discretization of the allowed wave vectors, standing-wave–like wave functions are obtained. In the vicinity of the HOMO and LUMO states, in particular, the local density of states (DOS) is modulated along the nanotube axis by $\sin^2(2\pi x/3a_0)$ or $\cos^2(2\pi x/3a_0)$ envelopes, with $a_0 = 0.25$ nm the lattice period. The resulting period of oscillation of the local DOS, $3a_0 = 0.75$ nm, has been observed experimentally by STS on a 30-nm-long single-wall nanotube.[9] A part of our present study is to provide a theoretical background for the interpretation of these experimental data. In particular, maps of the STS differential conductance directly comparable to experiment are provided. This communication also aims at predicting the STS signature of a pentagon-heptagon pair defect whose observation still remains challenging to the experiment.

A general, first-order perturbation expression of the tunneling current between the tip (t) and the substrate (s) has been derived in a tight-binding description:[12,14]

$$\mathcal{I} = (2\pi)^2 \frac{e}{\hbar} \sum_{I,I'} \sum_{J,J'} v_{IJ} v_{I'J'} \mathcal{I}_{II'JJ'},$$

$$\mathcal{I}_{II'JJ'} = \int_{-eV}^{0} dE\, n^t_{II'}(E^t_F + eV + E)\, n^s_{JJ'}(E^s_F + E). \quad (1)$$

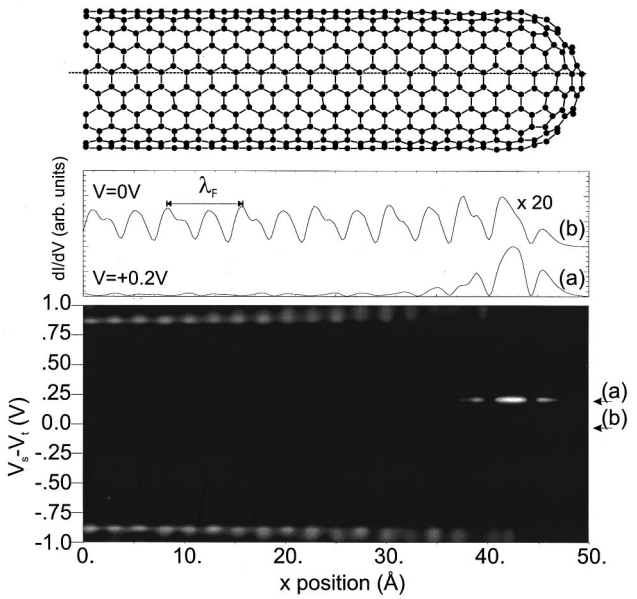

FIG. 1. STS computation on a long capped (10,10) tube (system I). Top: portion of tubule on which the computation was done, along a scan line visualized by the dashed line. Bottom: map representing dI/dV in gray scale against the tip x coordinate and the bias potential. Middle: linecuts labeled (a) and (b), representing dI/dV *versus* x for $V = -0.2$ V and $V = 0$ V, respectively.

 ©1999 The American Physical Society

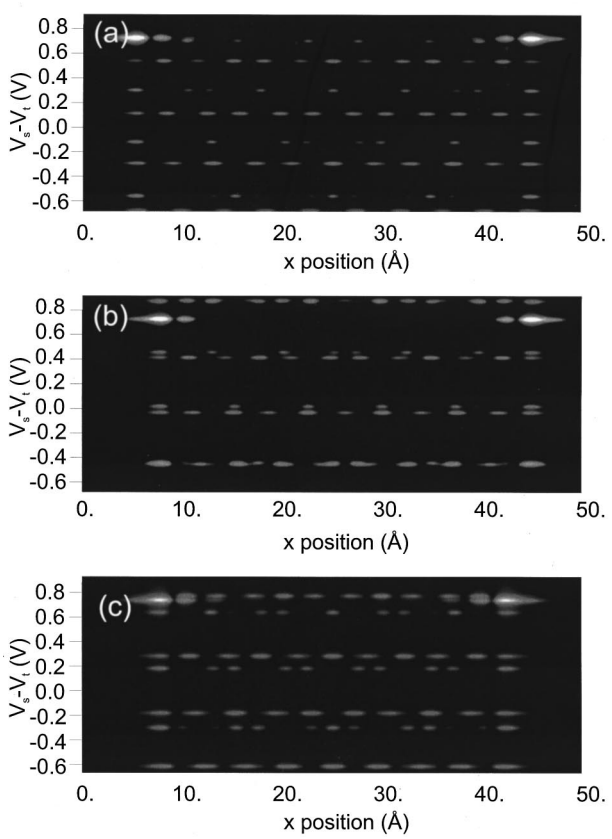

FIG. 2. STS gray-scale maps of tube II (a), III (b), and IV (c). The horizontal axis represents the tip position along the axis. The vertical axis shows the difference between the tube and the tip potential.

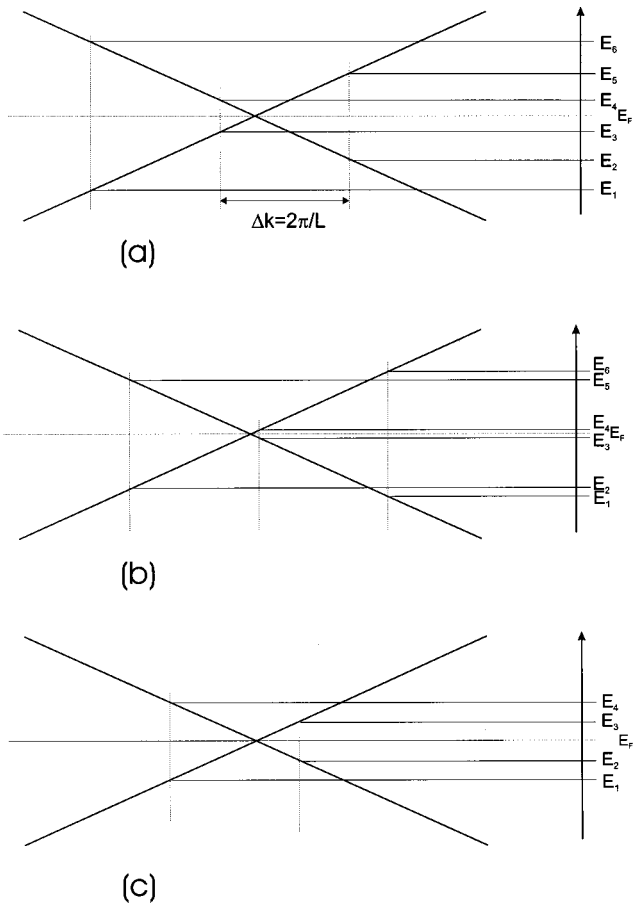

FIG. 3. Schematic electronic structure of tubes II, III, and IV. The relative spacings between the discrete states can be understood from the electronic structure of a straight infinite (5,5) tube. The 1D wave vector k can only take discrete values, with regular spacings $\sim 1/L$.

V is the tip-sample bias potential ($e>0$), the E_F's are the Fermi levels of the unperturbed systems, and v_{IJ} are the tip-sample coupling elements. Diagonal ($I'=I$) elements of $n^{\lambda}_{II'}(E)=\Sigma_{\beta\in\lambda}\psi^{\beta}_{I}{}^{*}\,\delta(E-E_\beta)\,\psi^{\beta}_{I'}$, where λ stands for t or s, respectively, represent the local densities of states on site I. When $I'\neq I$, $n_{II'}(E)$ describes the bonding or antibonding nature of the $I-I'$ bond. A discussion about this quantity is given in the appendix. The elements $n_{II'}(E)$ are computed as the imaginary part of the matrix element II' of the Green function. The tight-binding Hamiltonian matrix elements are given by Slater-Koster parameters restricted to π orbitals and first neighbor interactions ($V_{pp\pi}=-2.75$ eV).[15]

Experimentally, the discrete energy levels of a finite-size nanotube can be probed after the nanotube has been cut by applying a voltage pulse to the STM tip.[16] A $\sim$30-nm-long nanotube obtained in this way was then studied by STS.[9] According to topographical measurements, this carbon nanotube was identified as a (10,10) armchair one.

We have performed STS simulations on both capped tubules and connected nanotubes. Four armchair tubes have been examined: one long (10,10) nanotube and three small (5,5) nanotubes. Tube I has a length of 33.4 nm and is capped by two hemispherical caps (half C_{240}). The first (5,5) nanotube (tube II) has a length of 4.2 nm. Tube III and tube IV have been obtained by removing, respectively, one and two circumferential rings of hexagons from tube II. STS computation along a nanotube junction, namely the metal-semiconductor (12,0)/(11,0) (tube V) has also been considered. This junction is a connection between zigzag tubules realized with a single pair of fused pentagon and heptagon, aligned parallel to the axis.[17]

STS spectra were computed while scanning the tube along its axis at a constant tip-tube height of 5 Å. For each tip position, the current was computed from Eq. (1) for values of the tip-substrate potential, V_s-V_t, ranging from -1.0 V to $+1.0$ V. The derivative of the local current dI/dV is displayed on the bottom panel of Fig. 1 as a gray-scale image. In system I, Bloch states are reflected by the cap of the nanotube and form a standing wave pattern. At the Fermi energy, the period of the standing wave compatible with the lattice period (a_0) is the Fermi wavelength $\lambda_F=3a_0$ (7.5 Å). In the central panel of Fig. 1, curve (b) shows the λ_F period of dI/dV superimposed on a periodic function having the lattice period. This explains the superstructures observed in the interval λ_F, which reproduces the experimental data fairly well.[16] In particular, the double-peak structure of curve (b) (around $x=17$ Å, for example) can be qualitatively compared to that observed on STS spectra. The bias potential (0.2 V) of curve (a) shows an unoccupied state localized on the cap.[18] The corresponding local density of states rapidly decreases as one proceeds into the tube. In the bottom panel, the states at $\sim\pm 0.9$ V correspond to Van Hove singularities located on both sides of the metallic plateau of the density of

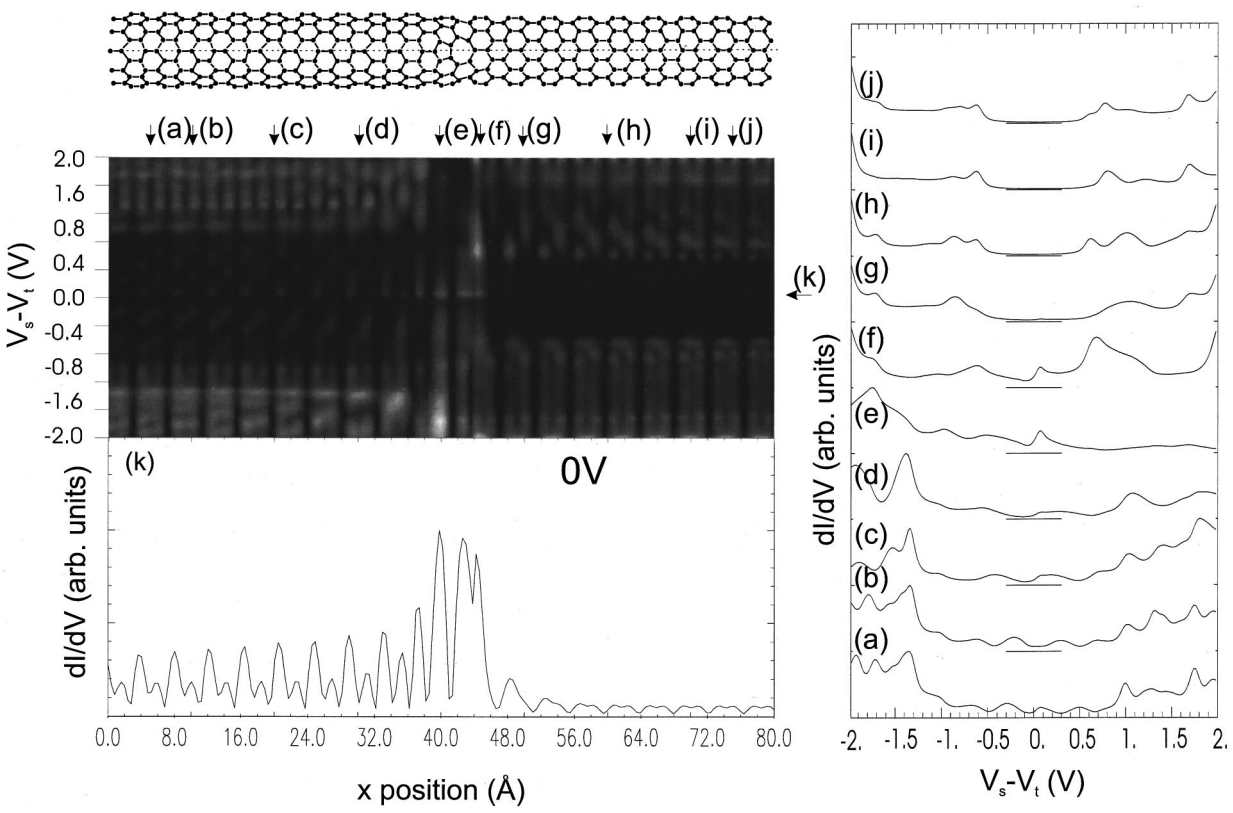

FIG. 4. STS computation on system V. The atomic structure is shown in the upper part of the figure. Gray-scale map of dI/dV as a function of the tip position and the bias potential is given in the central left part, with line, cuts along the vertical directions (a) to (j) (right panel), and for zero bias potential [curve (k), bottom].

states. At a distance of 40 Å from the tip, the bulk properties of the (10,10) nanotube are recovered.

Figure 2 represents the first derivative of the current computed along the tube axis of the short-length (5,5) tubules II, III, and IV [Figs. 2(a), 2(b), and 2(c), respectively]. The zero bias potential refers to the Fermi energy of each system, at the center of the HOMO-LUMO gap. Localized cap states at about 0.6 V are present in all cases. The extended states again present triple quasiperiod oscillations (7.5 Å) formed by standing-wave patterns. Despite geometrical similarities, the tubes II–IV clearly have different electronic structures. In the first approximation, the electronic structure of a nanotube of length L can be inferred from the band structure of the nonterminated system,[19] in particular from the two π and π^* bands crossing at the Fermi energy, by discretizing the Bloch wave vector k. The allowed k values are separated by $2\pi/L$. By changing the tube length by one lattice parameter a_0, the position of the k mesh moves by approximately one third of the discretization step.[19,20] The energy levels obtained from the sketch drawn at Figs. 3(a), 3(b), and 3(c) explain the electronic structure revealed by the STS data (Fig. 2). For instance, the HOMO-LUMO gap of tube III is almost closed because there is a k point close to the band crossing in Fig. 3(b). Adding or subtracting one circumferential ring of hexagons in the nanotube moves the corresponding k point to the left or to the right of the crossing point and this changes the HOMO-LUMO gap. These results, obtained here for capped tubes, agree with the calculations of Ref. 13 performed on open-end tubes.

The atomic structure shown in Fig. 4 displays the pentagon-heptagon connection between a (12,0) nanotube (left) and a (11,0) nanotube (right).[17] The structure has been scanned along the dotted line. The computed dI/dV map is shown in gray-scale on the central panel of the figure. One clearly sees the metallic plateau on the (12,0) side of the junction, located between -1.25 V and $+1.25$ V. The perturbation induced by the 5–7 defect introduces short-period oscillations in the densities of states.[21] These oscillations are also clearly visible on the bottom panel where the scan of dI/dV at zero bias potential has been represented. On the pentagon, the unoccupied part of the DOS is considerably reduced in favor of the occupied states which increase [curve (e)]. On the heptagon, the unoccupied states increased [curve (f)]. This can be explained with Hückel's rule: cyclic π-electron systems having 6, 10 . . . π electrons are the most stable ones. The five- and seven-membered rings will therefore tend to form 6-π-electron systems by charge transfers to stabilize the defect. The band gap of the semiconducting (11,0) nanotube formed right after the heptagon is enclosed by two Van Hove singularities at -0.6 V and $+0.6$ V. The curves (a)–(j) in the right panel of Fig. 4 show the dI/dV curves computed at the location indicated by the arrows (a)–(j) on the left-hand side. At these locations, the STM tip is located just above atomic sites of the structure.

We have used a tight-binding theory to perform STS calculation on carbon nanotubes, including capped and finite nanotubes, and one junction. The simulations are in qualitative agreement with experimental results obtained on a cut (10,10) tube. On the other hand, we have demonstrated that

weak modifications of the structure of finite-size nanotubes have strong influence on STS spectra. Finally, we have shown, using an example of a carbon nanotube junction, that odd-membered rings have a characteristic electronic signature, emphasizing the use of STS for pentagon or heptagon identification.

This work has been realized under the auspices of the Interuniversity Research Program on Systems of Reduced Dimensionality (PAI-IUAP N. P4 / 10) funded by the Belgian federal government. V.M. thanks the F.R.I.A and P.S., the F.N.R.S. for financial support.

APPENDIX: SEEING A BOND IN STM

Let us consider the tunneling currents $\mathcal{I}_{\text{bridge}(JJ')}$ and $\mathcal{I}_{\text{top}(J)}$ at the middle of the bond $J-J'$ and at the top of the atom J, respectively. These currents have contributions from all the interatomic tip-sample interactions. However, because the current between two sites decreases exponentially with the distance, the atoms closest to the tip give the major contribution to the current. When scanning along the bond JJ', the current is thus dominated by the contribution due to atoms J and J'. It follows that top and bridge currents can be approximately expressed by

$$\mathcal{I}_{\text{top}(J)} \approx (2\pi)^2 \frac{e}{\hbar} (v_{IJ}^t)^2 \mathcal{I}_{IIJJ}, \tag{A1}$$

and

$$\mathcal{I}_{\text{bridge}(JJ')} \approx (2\pi)^2 \frac{e}{\hbar} [2 v_{IJ}^b v_{IJ'}^b \mathcal{I}_{IIJJ'}] + \frac{\mathcal{I}_{\text{top}(J)} + \mathcal{I}_{\text{top}(J')}}{2}. \tag{A2}$$

In the last equation, we have assumed that the coupling parameters on the top positions and at the middle of the bond are identical before normalization of the tunneling probability. This is fully justified for small tip-sample distances of the order of 3 to 4 bond lengths. At weak and large bias potentials, the matrix elements $\mathcal{I}_{IIJJ}$ and $\mathcal{I}_{IIJJ'}$ have simple physical meanings. Assuming $|eV|$ small and the nonlocal density of states (NLDOS) constant on the small energy interval $|eV|$ around the Fermi levels, Eq. (1) gives

$$\mathcal{I}_{IIJJ'} \approx -eV n_{II}^t(E_F^t) n_{JJ'}^s(E_F^s), \tag{A3}$$

where $n_{II}^t(E_F^t) = |\psi_I^{F^t}|^2$ and $n_{JJ'}^s(E_F^s) = \psi_J^{F^s *} \psi_{J'}^{F^s}$ are LDOS and NLDOS at the Fermi level of the tip and sample, respectively. With $V>0$, $n_{II}^t(E_F^t)$ represents the LUMO density of the tip at site I, and $n_{JJ'}^s(E_F^s)$ is the HOMO of the sample at sites J and J'.

At large bias eV, most of the occupied states of the sample contribute to the current. Therefore, Eq. (1) involves the integration of the NLDOS of the sample over most of the occupied states:

$$\mathcal{I}_{IIJJ'} \approx u_I^t p_{JJ'}^s, \tag{A4}$$

where the quantity u_I^t represents a charge associated with the unoccupied levels of the tip and $p_{JJ'}^s = \Sigma_\beta^{occ} \psi_J^{\beta *} \psi_{J'}^\beta$ is the well-known bond order associated with the pair JJ'.[22]

From this discussion, we see that the tunneling current is controlled by the frontiers orbitals at low bias [Eq. (A3)] and by the charges and bond order at high bias [Eq. (A4)].

[1] S. Iijima, Nature (London) **354**, 56 (1991).
[2] C. Dekker, Phys. Today **52**, 22 (1999).
[3] C. Lieber, Solid State Commun. **107**, 607 (1998).
[4] M. Terrones *et al.*, Top. Curr. Chem. **199**, 189 (1999).
[5] J. Wildoer *et al.*, Nature (London) **391**, 59 (1998).
[6] T.W. Odom *et al.*, Nature (London) **391**, 62 (1998).
[7] P. Kim *et al.*, Phys. Rev. Lett. **82**, 1225 (1999).
[8] A. Hassanien *et al.*, Appl. Phys. Lett. **73**, 3839 (1998).
[9] L. Venema *et al.*, Science **283**, 52 (1999).
[10] A. Rubio, Appl. Phys. A: Mater. Sci. Process. **68A**, 275 (1999).
[11] D. Carroll *et al.*, Phys. Rev. Lett. **78**, 2811 (1997).
[12] V. Meunier *et al.*, Phys. Rev. Lett. **81**, 5588 (1998).
[13] A. Rubio *et al.*, Phys. Rev. Lett. **82**, 3520 (1999).
[14] M. Tsukada *et al.*, J. Phys. Soc. Jpn. **56**, 2875 (1987).
[15] J. C. Slater *et al.*, Phys. Rev. **94**, 1498 (1954).
[16] L. Venema *et al.*, Appl. Phys. Lett. **71**, 2629 (1997).
[17] R. Saito *et al.*, Phys. Rev. B **53**, 2044 (1996).
[18] P. Lambin *et al.*, J. Phys. Chem. Solids **58**, 1833 (1997).
[19] H.-Y. Zhu *et al.*, J. Phys. Chem. Solids **59**, 417 (1998).
[20] V. Meunier *et al.*, Phys. Rev. B **57**, 14 886 (1998).
[21] T. Kostyrko *et al.*, Phys. Rev. B **59**, 3241 (1999).
[22] J.N. Murrell *et al.*, *The Chemical Bond* (John Wiley and Sons, Chichester, NY, 1978).